# Reanalysis of NOAA $H_2$ observations: implications for the $H_2$ budget

Fabien Paulot[1], Gabrielle Pétron[2,3], Andrew M. Crotwell[2,3], and Matteo B. Bertagni[4,5]

[1]Geophysical Fluid Dynamics Laboratory, National Oceanic and Atmospheric Administration, Princeton, NJ, USA
[2]Cooperative Institute for Research in Environmental Sciences, University of Colorado Boulder, Boulder, CO, USA
[3]Global Monitoring Laboratory, National Oceanic and Atmospheric Administration, Boulder, CO, USA
[4]High Meadow Environmental Institute, Princeton University, Princeton, NJ, USA
[5]Department of Civil and Environmental Engineering, Princeton University, Princeton, NJ, USA

**Correspondence:** Fabien Paulot (fabien.paulot@noaa.gov)

**Abstract.** Hydrogen ($H_2$) is a promising low-carbon alternative to fossil fuels for many applications. However, significant gaps in our understanding of the atmospheric $H_2$ budget limit our ability to predict the impacts of greater $H_2$ usage. Here we use NOAA $H_2$ dry air mole fraction observations from air samples collected from ground-based and ship platforms from 2010 to 2019 to evaluate the representation of $H_2$ in the NOAA GFDL-AM4.1 atmospheric chemistry-climate model. We find that the base model configuration captures the observed interhemispheric gradient well but underestimates the surface concentration of $H_2$ by about 10 ppb. Additionally, the model fails to reproduce the 1-2 ppb/year mean increase in surface $H_2$ observed at background stations. We show that the cause is likely an underestimation of current anthropogenic emissions, including potential leakages from $H_2$-producing facilities. We also show that changes in soil moisture, soil temperature, and snow cover have likely caused an increase in the magnitude of the soil sink, the most important removal mechanism for atmospheric $H_2$, especially in the Northern Hemisphere. However, there remains uncertainty due to fundamental gaps in our understanding of $H_2$ soil removal, such as the minimum moisture required for $H_2$ soil uptake, for which we performed extensive sensitivity analyses. Finally, we show that the observed meridional gradient of the $H_2$ mixing ratio and its seasonality can provide important constraints to test and refine parameterizations of the $H_2$ soil sink.

## 1 Introduction

Increased hydrogen ($H_2$) usage has been proposed as a strategy to reduce the carbon intensity of many sectors of the economy that are difficult to electrify (Hydrogen Council, 2017; da Silva Veras et al., 2017; Staffell et al., 2019; Abe et al., 2019; Dawood et al., 2020). The climate benefits of greater $H_2$ usage depend primarily on the $H_2$ production pathway. Current $H_2$ production is dominated by steam reforming of methane ($CH_4$) in natural gas (Holladay et al., 2009; International Energy Agency, 2019), a process that is very carbon intensive (Howarth and Jacobson, 2021). Carbon capture can reduce $CO_2$ emissions associated with $H_2$ production. However, methane leakage throughout the supply chain could offset much of the expected climate benefits of increased $H_2$ usage (Howarth and Jacobson, 2021; Ocko and Hamburg, 2022; Bertagni et al., 2022; Hauglustaine et al., 2022). Alternative production pathways such as renewable-based electrolytic $H_2$ can provide large and rapid reductions in radiative

forcing (Hauglustaine et al., 2022), and considerable investments have been devoted to reducing their cost (International Energy Agency, 2022). Furthermore, evidence of significant concentrations of $H_2$ in surface and subsurface natural gases (Zgonnik, 2020; Milkov, 2022; Lefeuvre et al., 2021) have spurred interest in the potential of naturally occurring $H_2$ as a new primary energy source (Prinzhofer et al., 2018; Lapi et al., 2022).

$H_2$ photooxidation in the atmosphere also tends to increase $CH_4$, $O_3$, and stratospheric water vapor, which results in indirect radiative forcing (Derwent et al., 2001; Paulot et al., 2021). Sand et al. (2023) recently calculated that $H_2$ has a global warming potential of $\simeq 11.6 \pm 2.8$ and $37.3 \pm 15.1$ for a 100 and 20-year time horizon, respectively.

Significant uncertainties regarding the overall budget of $H_2$ remain. $H_2$ sources include both emissions and photochemical production from the oxidation of volatile organic compounds (VOCs). Estimates for the overall source of atmospheric $H_2$ range from $\simeq 70$ to 110 Tg/yr, a large spread primarily associated with the magnitude of the $H_2$ photochemical sources (Ehhalt and Rohrer, 2009). Recent work also argues that current estimates of $H_2$ sources need to be revised upward to account for geologic $H_2$ seepage (Zgonnik, 2020). These uncertainties in the nature and magnitude of $H_2$ sources have proved challenging to reduce in part because of commensurate uncertainties in $H_2$ sinks. The atmospheric oxidation of $H_2$ by OH is well understood but is estimated to account for less than one third of the overall atmospheric sink (Ehhalt and Rohrer, 2009; Paulot et al., 2021). The most important removal pathway is the consumption of $H_2$ by high-affinity hydrogen oxidizing bacteria (HA-HOB), a class of bacteria that have been identified in many different soils (Constant et al., 2008; Greening et al., 2015; Bay et al., 2021; Greening and Grinter, 2022). Several parameterizations of the $H_2$ soil sink have been developed (Ehhalt and Rohrer, 2013; Price et al., 2007; Smith-Downey et al., 2006; Bertagni et al., 2021) that aim at capturing the observed sensitivity of $H_2$ soil removal to soil temperature, soil moisture and ecosystem/soil type (Ehhalt and Rohrer, 2009). However, observational constraints on $H_2$ soil removal remain very limited (Meredith et al., 2016) and this process remains challenging to represent in global models (Yashiro et al., 2011; Paulot et al., 2021).

Here, we leverage the recently completed recalibration of $H_2$ measurements collected by NOAA Global Monitoring Laboratory to perform a comprehensive evaluation of the simulation of $H_2$ in the Geophysical Dynamics Laboratory (GFDL) AM4.1 model (Horowitz et al., 2020; Paulot et al., 2021). The NOAA monitoring network provides additional spatial coverage that complements other existing networks (AGAGE (Prinn et al., 2018), CSIRO (Francey et al., 2003)) and offers a unique opportunity to evaluate the skill of the model in capturing changes in $H_2$ atmospheric concentration since 2010. This period is especially important to gain a quantitative understanding of the present-day $H_2$ budget, also given that recent $H_2$ observations at Mace Head (Derwent et al., 2021, 2023) show both an increase in $H_2$ concentration and its soil removal rate. The study is organized as follows: we first describe and evaluate the representation of $H_2$ in the GFDL-AM4.1 global chemistry-climate model, focusing on changes in $H_2$ over the 2010–2019 period. We then assess the sensitivity of the $H_2$ simulations to uncertainties in the $H_2$ budget focusing on the representation of anthropogenic $H_2$ emissions and soil removal.

## 2 Methods

### 2.1 Observations

NOAA Global Monitoring Laboratory (GML) provides long-term monitoring of long-lived greenhouse gases and other trace species. The NOAA GML Global Cooperative Air Sampling Network is a partnership between GML and many outside organizations and individual volunteers to collect discrete air samples approximately weekly from 60+ globally distributed sites (Global Monitoring Laboratory, 2023). These sites are often situated to collect air representative of large regional air masses. Priorities are placed on sites where opportunities exist for local support which can be maintained over long (decadal) time scales. The discrete air samples are collected weekly in pairs of 2 L glass flasks and are returned to GML for measurements of multiple species on central measurement systems thus providing a high level of consistency across the globally distributed network.

GML measurements of $H_2$ in the discrete air samples began in the late 1980's as an opportunistic measurement associated with the analytical technique then used for measuring atmospheric carbon monoxide (CO). To facilitate these $H_2$ measurements, NOAA/GML developed an in-house $H_2$-in-air reference scale based on a few gravimetric standards (the latest iteration named H2-X1996). This reference scale was not stable over time and introduced significant time-dependent measurement errors. GML recently converted part of the historical $H_2$ measurement records to the $H_2$ calibration scale recommended by the World Meteorological Organization (WMO/MPI H2-X2009) maintained by Max Planck Institute (MPI) in Jena, Germany (Jordan and Steinberg, 2011). Measurements since approximately 2010 have been reprocessed onto the MPI scale to remove the biases inherent in the NOAA X1996 scale (Pétron et al., submitted). NOAA reprocessed $H_2$ data since 2010 is consistent to within 1-2 ppbv on an annual basis for same air measurements with CSIRO and the MPI-BGC (Pétron et al., submitted). However, earlier NOAA data that remains on the obsolete NOAA X1996 scale is known to be biased relative to the later NOAA data and to other monitoring programs.

Here, we only consider ground stations from the NOAA cooperative air sampling network with at least 96 distinct monthly observations over the 2010-2019 period (80% coverage, Fig. S1). Ship-based observations are binned in 4°x4° regions and we only consider regions with at least 40 observations.

### 2.2 Model setup

We use the GFDL Atmospheric Chemistry Model AM4.1 (Horowitz et al., 2020). For all configurations, the model is run from 2004 to 2019. Monthly sea surface temperature and sea ice concentration are from Rayner et al. (2003) and Taylor et al. (2000). Horizontal winds are nudged to 6-hourly horizontal winds from the National Center for Environmental Prediction (Kalnay et al., 1996). The model output is sampled at the time and location of the air sampling. To better quantify the drivers of the $H_2$ distribution and trend, we tag $H_2$ associated with anthropogenic, marine, soil, and biomass burning direct $H_2$ emissions and $H_2$ produced by the oxidation of VOCs.

## 2.2.1 BASE simulation

AM4.1 includes a detailed representation of $H_2$ (Paulot et al., 2021), which is briefly summarized here. This configuration will be referred to as BASE (Table 1), hereafter. $H_2$ sources include both direct emission from anthropogenic and natural sources as well as photochemical production. Anthropogenic emissions of $H_2$ ($\simeq$ 13 Tg/yr over the 2010–2019 period) are estimated from CO emissions in the Community Emissions Data System (CEDS) v20210421 (O'Rourke et al., 2021) using time-invariant sector–specific emission $H_2$:CO emissions ratios (Table S1). The transportation and residential sectors are the largest contributors to anthropogenic $H_2$ emissions (Fig. S2). Biomass burning emissions ($\simeq$ 8 Tg/yr) are estimated using the Global Fire Emissions Database (GFED4s, van der Werf et al. (2017)) with emission factors from Akagi et al. (2011) and Andreae (2019). Marine (6 Tg/yr) and terrestrial (3 Tg/yr) sources of $H_2$ are prescribed as a monthly climatology and distributed spatially (Fig. S3) based on the soil and marine CO emission patterns in the Precursors of Ozone and their Effects in the Troposphere inventory (Granier et al., 2005). The BASE emission inventory does not include geological sources of $H_2$.

The production of $H_2$ associated with $CH_2O$ photolysis is calculated interactively using FAST-JX version 7.1, as described by Li et al. (2016). Formaldehyde sources are dominated by the oxidation of VOCs from anthropogenic (O'Rourke et al., 2021), biomass burning (van der Werf et al., 2017), and natural origins. Biogenic emissions of VOCs are prescribed as a monthly climatology (Granier et al., 2005), except for isoprene and terpenes, of which emissions are calculated interactively using the Model of Emissions of Gases and Aerosols from Nature (Guenther et al., 2012). Surface $CH_4$ is prescribed as a monthly latitudinal profile from observations up to 2014 (Meinshausen et al., 2017) and from the SSP1-2.6 scenario after 2015 (Meinshausen et al., 2020). We select this scenario as it tracks well the observed global $CH_4$ surface mixing ratio from the World Meteorological Organization Global Atmospheric Watch greenhouse gases observational network (WMO, 2021). To characterize the contribution of different VOC emissions to the photochemical production of $H_2$, we perform a set of sensitivity experiments in which we perturb the emission of a given VOC by 10% and quantify the response of $H_2$ production. For $CH_4$ oxidation, we directly track the different oxidation pathways that result in $H_2$ production. The molar yield of $H_2$ from $CH_4$, isoprene, methanol, and terpene are estimated to be 0.38, 0.57, 0.21, and 0.66 mol/mol, respectively. These yields are broadly similar to estimates derived by Ehhalt and Rohrer (2009) (0.37, 0.54, 0.19, 0.71, respectively) but are lower than estimates derived from box-model (0.38, 0.83, 0.38, and 0.85, respectively for $NO_x$=160 pptv (Grant et al., 2010)), which may reflect the impact of wet and dry deposition. In particular, Fig. S4 shows that the simulated yield of $H_2$ from $CH_4$ oxidation is lowest in the tropics, where most $CH_4$ is oxidized, as a greater fraction of $CH_2O$ is oxidized by OH in this region than at high latitudes.

Overall, we find that $CH_4$ oxidation is the largest photochemical source of $H_2$ ($\simeq$27 Tg/yr). The oxidation of biogenic VOCs (BVOCs) accounts for the majority of the remaining photochemical source of $H_2$ ($\simeq$ 14 Tg/yr) primarily from isoprene (8 Tg/yr), methanol (3 Tg/yr), and terpene (1 Tg/yr). The oxidation of VOCs from anthropogenic and biomass burning origin produces $\simeq$3 Tg/yr of $H_2$. Our estimates are in good agreement with previous estimates (Ehhalt and Rohrer, 2009): $CH_4$ ($23\pm8$ Tg/yr), isoprene ($9\pm6$ Tg/yr), biomass burning and anthropogenic VOCs (3 Tg/yr). This similarity can attributed to the similar yield of $H_2$ from $CH_2O$ (0.4 mol/mol compared to 0.37 (Ehhalt and Rohrer, 2009)). More work is needed to better characterize the temperature and pressure sensitivity of $CH_2O$ photolysis quantum yields (Röth and Ehhalt, 2015).

Fig. 1a summarizes the simulated sources of $H_2$ associated with photochemical production and direct emissions in the BASE run. Over the 2010-2019 period, the average global simulated source of $H_2$ is $74\pm1$ Tg/yr, with 60% from photochemical production. Anthropogenic activities are estimated to account for $\simeq 40\%$ of the overall $H_2$, primarily from the $CH_4$ oxidation. Note that we assume that 50% of the photochemical production of $H_2$ from $CH_4$ oxidation is anthropogenic based on the detailed bottom-up inventory of $CH_4$ sources (Saunois et al., 2020). Top-down estimates suggest a higher contribution of anthropogenic sources ($\simeq 60\%$, Saunois et al. (2020)), which would further increase the fraction of $H_2$ associated with anthropogenic activities. Fig. 1b shows that the simulated total source of $H_2$ changes little over the 2010–2019 period. The simulated annual photochemical source of $H_2$ is 1.6 Tg/yr greater in 2017-2019 than in 2010-2012, with 70% of this increase attributed to $CH_4$. In contrast, $H_2$ associated with anthropogenic activities decreases (-1.3 Tg/yr, Fig. S2a), mostly from transport (-1 Tg/yr) and industries (-0.4 Tg/yr). The decrease in $H_2$ emissions reflects the decline in CO emissions from these sectors. The interannual variability of the overall $H_2$ source over the 2010-2019 period is dominated by the variability of biomass burning emissions, which can result in interannual changes of $\simeq 2$ Tg/yr.

$H_2$ sinks include chemical oxidation by OH and O($^1$D), and soil uptake associated with microbial activity. The deposition velocity of $H_2$ ($v_d(H_2)$) over land is calculated following the parameterization of Ehhalt and Rohrer (2013) and depends on temperature, soil moisture (Ehhalt and Rohrer, 2013) and soil carbon (Khdhiri et al., 2015; Paulot et al., 2021). In the BASE configuration we use a monthly climatology of $v_d(H_2)$ calculated using monthly meteorological and soil outputs from the GFDL Earth System Model ESM4.1 over the 1989–2014 period (Dunne et al., 2020; Paulot et al., 2021). Soil uptake is estimated to account for 71% of the overall $H_2$ sink. The overall lifetime of $H_2$ in the BASE configuration is 2.5 years. The lifetime of $H_2$ associated with anthropogenic emissions is 6% shorter due to their geographical distribution.

### 2.2.2   Sensitivity simulations

In this section, we describe additional model simulations that are designed to explore the impact of uncertainties in the representation of $H_2$ emission and deposition on the simulation of atmospheric $H_2$ (Table 1). We focus on $H_2$ emissions and deposition as their representations in models are largely derived from limited observational constraints (Derwent et al., 2023; Paulot et al., 2021).

The REVISED configuration focuses on the representation of anthropogenic and natural $H_2$ emissions. The development of the REVISED emission inventory is guided by the biases of the BASE configuration against $H_2$ observations (Supporting materials S1.1, Ghosh et al. (2015)). In particular, we focus on the representation of transportation emissions (Table S1) and emissions associated with industrial $H_2$ use for refining, ammonia, methanol and steel production. Further details regarding the treatment of anthropogenic and natural sources in the REVISED emission inventory can be found in the Supporting materials (Texts S1.2 and S1.3)

We further consider the impact of a different representation of $H_2$ soil uptake on the simulation of $H_2$. Here, we use the parameterization of the soil moisture response of HA-HOB activity recently developed by Bertagni et al. (2021). This parameterization relates the minimum soil moisture required for $H_2$ uptake by HA-HOB to soil hydrological properties, which facilitates its incorporation in global models. This model also allows to vary the strength of the diffusion barrier associated with
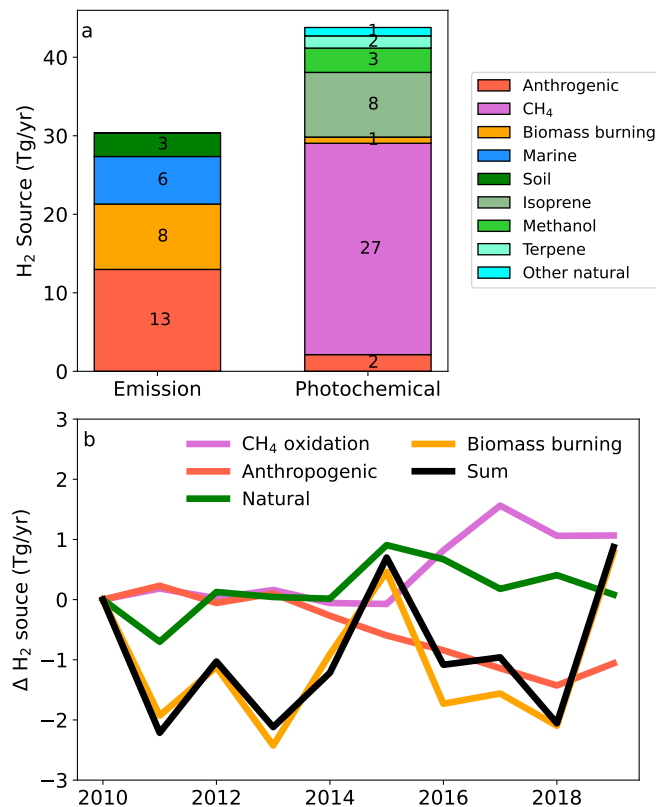
**Figure 1.** Global source of $H_2$ (panel a). Panel b shows the changes in the magnitude of $H_2$ sources over the 2010–2019 period. For clarity, the green line denotes the combined change in $H_2$ emissions and photochemical production from natural sources (marine and soil emissions + BVOCs photooxidation).

soil litter, which can reduce $H_2$ transport to active sites (Smith-Downey et al., 2008; Ehhalt and Rohrer, 2009). To quantify possible changes in $v_d(H_2)$ over the 2010-2019 period, we calculate daily deposition velocity using 3-hourly soil moisture, soil temperature, and snow cover from the NASA Global Land Data Assimilation System (Rodell et al., 2004). We focus on two different configurations. In REVISED_GLDAS, we neglect the litter resistance and assume that HA-HOB activity is inhibited when the soil matrix potential ($\Psi_{ws}$) is less than the wilting point of plants in semiarid environments ($\Psi_{ws} = -3000$ kPa) as recommended by Bertagni et al. (2021). The required soil moisture for the $H_2$ uptake is not well known and experimental studies have shown that HA-HOB are present in very arid environments (Jordaan et al., 2020). In REVISED_GLDAS2, we assume a much lower activation threshold for HA-HOB ($\Psi_{ws} = -10,000$ kPa) and account for the litter barrier. Note that both these configurations use the REVISED emission inventory. More details regarding the calculation of $v_d(H_2)$ can be found in the Supporting materials (Text S1.4).

**Table 1.** Model configurations

| | H$_2$ anthropogenic emission | H$_2$ natural emission | H$_2$ soil removal |
|---|---|---|---|
| **BASE** | Time-invariant H$_2$:CO emission ratio (Table S1) | Ocean+Soil: Monthly climatology<br>Biomass burning: GFED4s | Monthly climatology $v_d$(H$_2$)<br>(Paulot et al., 2021) |
| **REVISED** | Revised H$_2$:CO emission ratio<br><br>Emission from industrial H$_2$ use<br>(Text S1.2 and Table S1) | Ocean: Calculated from CO seawater concentration<br>Soil: Calculated from N fixation<br>(Text S1.3)<br>Biomass burning: same as BASE | Same as BASE |
| **REVISED_GLDAS** | same as REVISED | Same as REVISED | Daily $v_d$(H$_2$) calculated using land reanalysis with soil moisture sensitivity from Bertagni et al. (2021)<br>(Text S1.4) |
| **REVISED_GLDAS2** | same as REVISED | Same as REVISED | Same as REVISED_GLDAS with canopy+litter resistance and a lower HA-HOB water-activation threshold<br>(Text S1.4) |

## 3 Results and discussion

### 3.1 BASE model evaluation

#### 3.1.1 Climatology

Fig. 2 shows the average model bias against surface observations from NOAA GML. In the BASE configuration, AM4.1 underestimates H$_2$ at all stations, with greater biases over continental regions (Fig. 2). Correlations exceed 0.5 at more than 90% of background sites (square) but only at 55% of continental sites. Fig. 2b further shows that the concentration at the South pole is $\simeq$ 50 ppb greater than at the North pole, which is well captured by the BASE configuration.

To examine differences between the model and observed seasonality, we first apply the Kmean++ clustering algorithm (Arthur and Vassilvitskii, 2007) to the observed H$_2$ monthly climatology. Since our focus is on the seasonality of H$_2$ we transform the monthly climatology of H$_2$ at each site such that it has a mean of 0 and a standard deviation of 1. Using the within-cluster sum of squares and the silhouette score, we find that the standardized H$_2$ observations can be well represented using 4 clusters. Fig. 3 shows the seasonality of the standardized H$_2$ concentration for each cluster (panel a) as well as their spatial distribution (panel b). Sites are found to cluster broadly by latitude based on the seasonality of H$_2$ with clusters 1, 2, 3, and 4 being comprised primarily of sites located in the Southern mid to high latitudes, Southern tropics, Northern subtropics, and Northern mid to high latitudes, respectively. The model captures the seasonality of H$_2$ well in the Southern Hemisphere (cluster 1) but peaks 1 to 3 months earlier than observations for clusters 2, 3 and 4. Fig. 3c shows the contribution of different
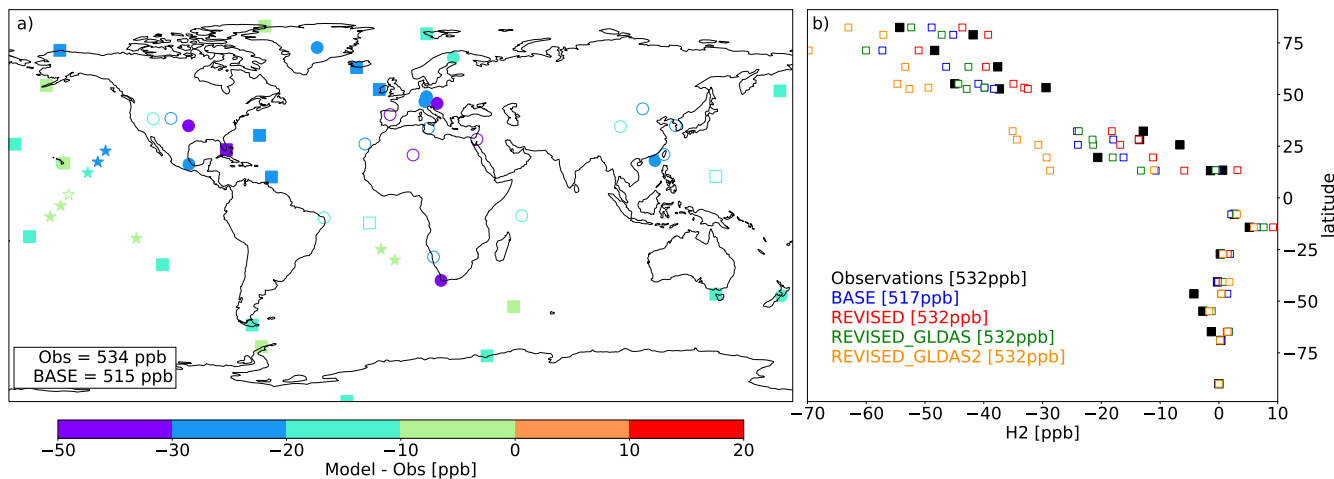
**Figure 2.** Mean model bias at individual sites for the BASE model configuration (a) over the 2010–2019 period. Filled symbols denote sites where the correlation between observed and simulated $H_2$ concentrations exceeds 0.5. Square and star symbols denote background sites and cruises, respectively. Panel (b) shows the observed and simulated difference in $H_2$ at background sites relative to $H_2$ mole fraction measured at the South Pole observatory. The average concentrations at background sites is indicated for each configuration in the legend.

sources of $H_2$ to the simulated seasonality of $H_2$ (inferred from the tagged $H_2$ tracers). The seasonal bias for cluster 2 is
180 primarily driven by $H_2$ emitted from biomass burning, which peaks $\sim$ 2 months earlier than observations. This delay may be associated with greater burning of woody material towards the end of the dry season, emitting more incompletely oxidized products such as $H_2$ (van der Werf et al., 2006). Fig. 3c also shows that the seasonal bias in clusters 3 and 4 may be associated with $H_2$ emitted by anthropogenic activities. As we will show in section 3.2.2, this seasonal bias may also reflect errors in the removal of $H_2$.

### 185 3.1.2 Time series

Fig. 4 shows that $H_2$ has increased at most sites with an average trend at background sites of 1.4$\pm$0.7 ppb/yr over the 2010-2019 period with little variability with latitude. Trends are calculated using ordinary least-square regression applied to the deseasonalized monthly $H_2$ concentrations. In contrast, simulated $H_2$ concentration in the BASE configuration changes little over this time period.

190 In the Northern hemisphere, the lack of trend at background sites in the model (Fig. 4c) reflects the near-cancellation between the increase of photochemically-produced $H_2$ and the decrease of $H_2$ emitted from anthropogenic sources, consistent with the changes in anthropogenic emissions and the photochemical source of $H_2$ from $CH_4$ and biogenic VOCs oxidation (Fig. 1). The simulated absolute trend in anthropogenic hydrogen is $\simeq$ 50% lower in the Southern Hemisphere relative to the Northern Hemisphere due to the higher relative areal density of anthropogenic sources in the Northern Hemisphere. In
195 contrast, the change in photochemically-produced $H_2$ exhibits little variability with latitude and matches the observed trend
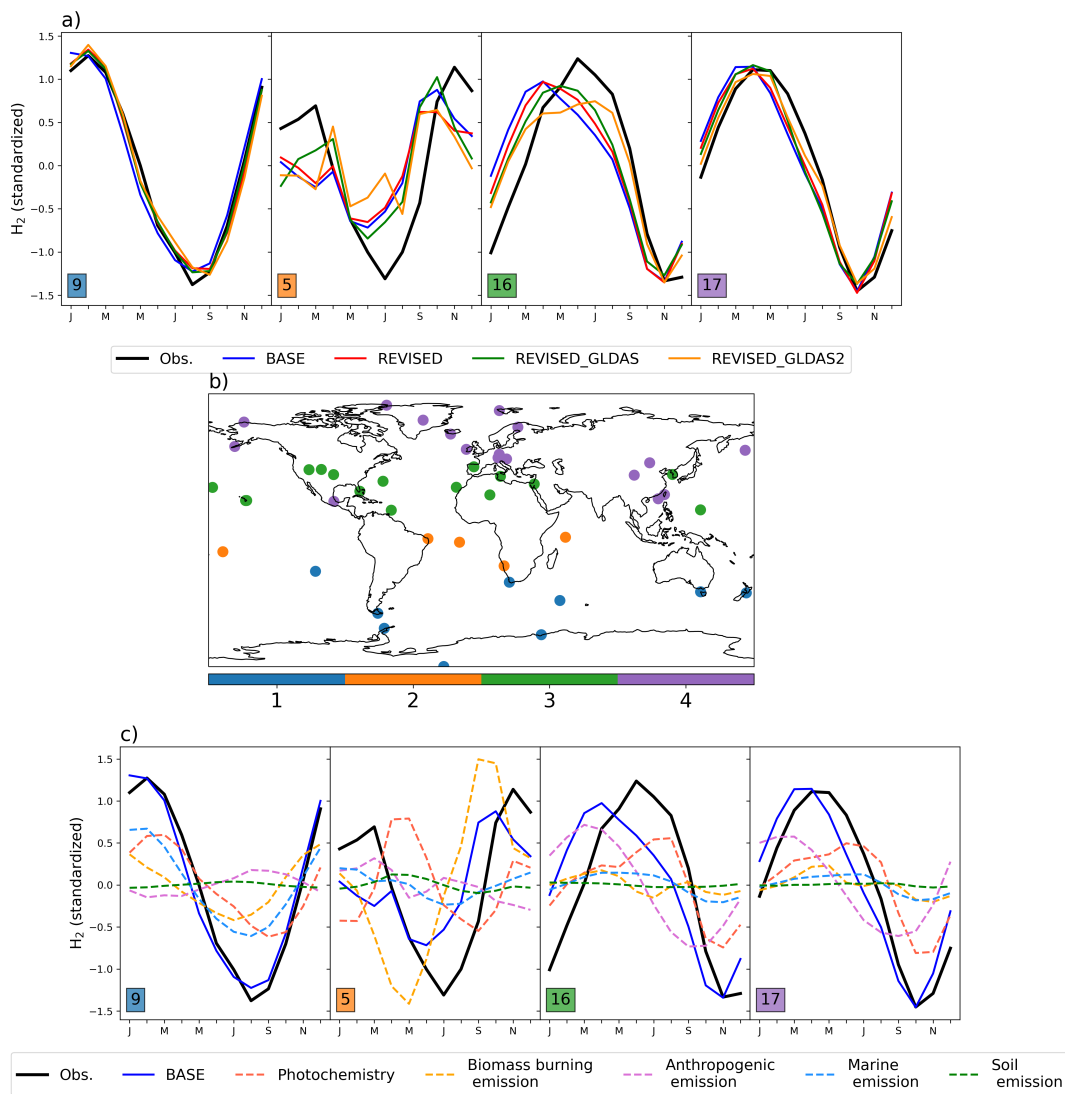
**Figure 3.** Monthly standardized $H_2$ concentration for each cluster (a). The number of sites in each cluster is indicated by insets. The sites included in each cluster are shown in panel (b). The variation of source-tagged $H_2$ tracers in each cluster is shown in panel (c). Source-tagged $H_2$ tracers are normalized using the standard deviation of simulated $H_2$.

well. The simulated trend also shows little latitudinal variation due to a decrease in $H_2$ from biomass burning in the Southern Hemisphere.
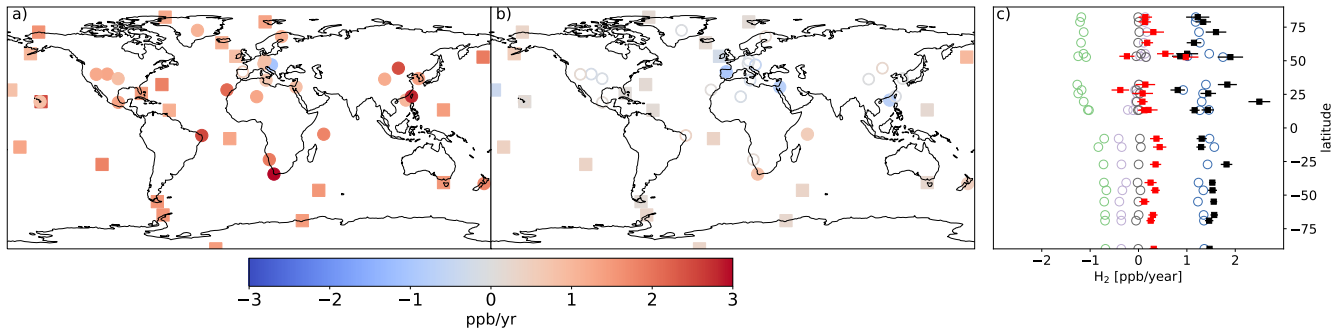
**Figure 4.** Trend in $H_2$ concentrations in observations (a) and in the BASE simulation (b) over the 2010–2019 period. Panel (c) shows the observed (black) and simulated (red) trend in $H_2$ at background sites (squares) as well as the trend in tagged $H_2$ tracers associated with anthropogenic sources (green), biomass burning (purple), ocean+soil sources (black), and photochemical production (blue). Filled symbols denote trends that are significantly different from 0 (p<0.01). The error bars show one standard deviation for the estimated observed and simulated trends.
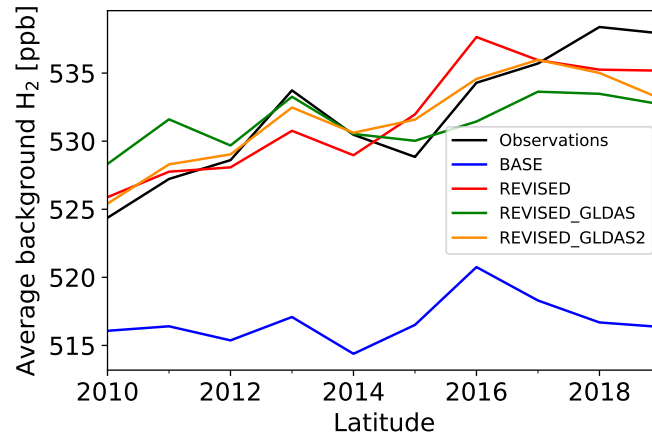
**Figure 5.** Mean observed and simulated $H_2$ at background sites (see Fig. 2 for locations)

## 3.2 Sensitivity simulations

In this section, we explore how uncertainties in the representation of $H_2$ emissions and deposition contribute to the biases in the BASE model run.

### 3.2.1 Emission

Fig. 5 shows that the BASE run exhibits a 10-15 ppb negative bias and fails to capture the $\simeq$ 15 ppb increase over the 2010–2019 period (Fig. 5). From this bias, we estimate a missing source of $H_2$ of $\simeq$ 2-2.5 Tg/yr circa 2010 and 3-4 Tg/yr circa
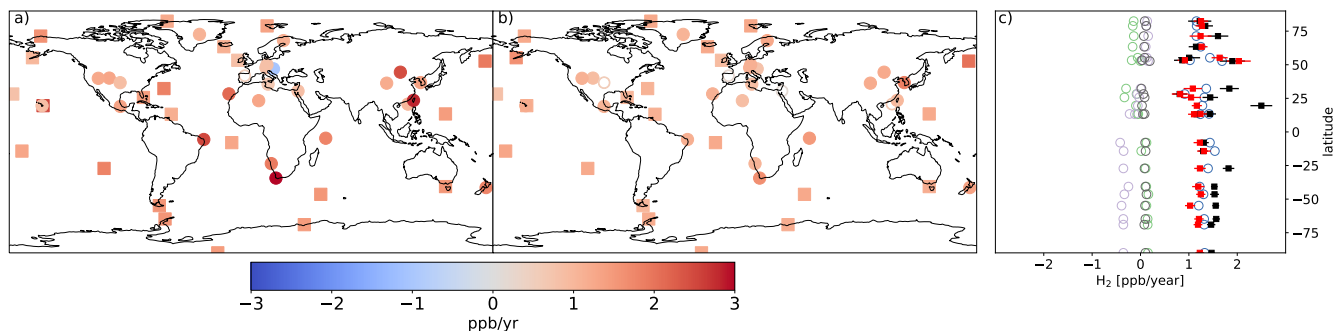
**Figure 6.** Same as Fig. 4 but for the REVISED configuration

2019 (Text S1.1). Similarly, Derwent et al. (2023) recently reported that a missing $H_2$ source (5 Tg/yr in 2020) was required to explain the observed increase in $H_2$ concentration at Mace Head and Cape Grim since 2010.

Figs 5 and 6 show that the observed increase in $H_2$ can be well captured with the REVISED emission inventory. In this inventory, the increase in the missing source of $H_2$ is explained by a lower decrease in anthropogenic $H_2$ emissions associated with fossil fuel combustion (0.9 Tg/yr lower in 2019 relative to 2010 compared to 1.6 Tg/yr in the BASE inventory) and an increase in $H_2$ emissions associated with $H_2$ industrial usage (0.3 Tg/yr). We also increase the $H_2$ soil source from 3 to 4.5 Tg/yr to reduce the model negative bias. This change is well within the large uncertainties in the minor $H_2$ sources surveyed by Ehhalt and Rohrer (2009). In particular, it is a small fraction of the estimated geological source of $H_2$ (23±7 Tg/yr (Zgonnik, 2020)), which we do not account for here.

The REVISED emission inventory provides a possible explanation for the observed increase in atmospheric $H_2$. It highlights the importance of constraining $H_2$ emissions associated with $H_2$ industrial use, a sector that is expected to grow rapidly in coming decades.

### 3.2.2 Deposition

The BASE and REVISED experiments assume no interannual variability in $v_d(H_2)$. However, we have recently shown that climate change may cause an increase in $v_d(H_2)$ (Paulot et al., 2021). Recent analysis of observations at Mace Head also suggests that $v_d(H_2)$ has increased in recent decades (Derwent et al., 2021).

Fig. 7 shows that the REVISED_GLDAS and REVISED_GLDAS2 $v_d(H_2)$ exhibit different meridional distributions relative to the BASE configuration with faster removal in the subtropics and northern high latitudes but slower removal in the tropics. This reflects more efficient removal of $H_2$ in arid regions and slower removal in the tropics. These spatial differences are the largest for the REVISED_GLDAS2 configuration due to the activation of HA-HOB at a lower soil moisture. Fig. 7b further shows that $v_d(H_2)$ in the REVISED_GLDAS and REVISED_GLDAS2 configuration both increase over the 2010-2019 period in the Northern mid latitudes. This increase reflects drier and warmer conditions in Europe, the Western US as well as parts of Siberia, which result in faster biological uptake rates and promote $H_2$ diffusivity (Fig. S5). This mechanism may contribute

to the reported 1.2%/yr increase in $H_2$ deposition velocity at Mace Head from 1994 to 2020 (Derwent et al., 2021). Drier conditions in Australia trigger biotic limitations, which results in a large decrease in $H_2$ deposition velocity in the Southern mid latitudes in the REVISED_GLDAS configuration. In contrast, we find no significant suppression of $H_2$ uptake in Australia over this time period in the the REVISED_GLDAS2 configuration due a lower threshold for biotic limitation.

Changes to the spatial distribution of $v_d(H_2)$ and the increase in $H_2$ removal in the Northern mid latitudes (Fig. 7b) in REVISED_GLDAS result in a larger pole-to-pole difference in surface $H_2$ (Fig. 2) and a reduction in the simulated trend (Fig. 8) in the Northern mid to high latitudes. Both of these changes tend to degrade the model performance relative to the REVISED configuration. In contrast, the REVISED_GLDAS configuration better captures the timing of the $H_2$ maximum in the northern hemisphere (clusters 3 and 4, Fig. 3a).

Systematic assessment of the sensitivity of $v_d(H_2)$ to $\Psi_{ws}$ and the strength of the litter barrier is shown in Fig. 9. We find that a lower soil moisture threshold for HA-HOB activation (i.e., a lower $\Psi_{ws}$) favors $H_2$ removal in the Northern hemisphere relative to the Southern hemisphere (Fig. 9a) and results in a larger increase in $v_d(H_2)$ over the 2010–2019 period (Fig. 9b), especially in the Southern hemisphere (Fig. 9c). This suggests that a lower $\Psi_{ws}$ would tend to worsen the model performance in the absence of a litter barrier (given the REVISED emissions). The litter barrier tends to increase the importance of arid regions for $H_2$ removal. This makes $H_2$ uptake more susceptible to moisture inhibition, such that a stronger litter barrier tends to result in a lower increase of even a decrease in $v_d(H_2)$ over the 2010-2019 period. Under all scenarios, the litter barrier tends to increase the gradient in $v_d(H_2)$ between Northern and Southern hemispheres.

It is notable that no configuration results in little change in $v_d(H_2)$ without producing large and increasing gradients between the Northern and Southern hemispheres. As a result, our model cannot capture the observed trends, meridional gradient, and seasonality together given our REVISED estimate of $H_2$ emissions. This is illustrated by the REVISED_GLDAS2 configuration ($\Psi_{ws}$=-10000 kPa, Litter_scale=1), which is found to improve the simulated trend relative to the REVISED_GLDAS (not shown) and the simulated seasonality relative to the REVISED configuration (Fig. 3) but results in a large overestimate of the South/North meridional gradient (Fig. 2). This highlights the need for a more detailed representation of the factors that modulate $v_d(H_2)$ (Khdhiri et al., 2015) to help interpret changes in $H_2$ concentrations.

## 4  Conclusions

The recently released $H_2$ dry air mole fraction measurements from the NOAA Global Cooperative Air Sampling Network expand the spatial coverage of the WMO Global Atmospheric Watch observations. This offers the opportunity to assess the representation of the $H_2$ atmospheric budget in the state-of-the-art GFDL-AM4.1 global atmospheric chemistry climate model. Observations show that $H_2$ has increased on average by 1 to 2 ppb/year over the 2010-2019 period. This change can be explained by the increase in photochemically-produced $H_2$ (mostly from $CH_4$) provided direct anthropogenic $H_2$ emissions have remained stable during this time period. We hypothesize that this stability reflects the compensation between declining emissions associated with fossil fuel combustion (mostly from the transport sector) and increasing emissions associated with $H_2$-producing facilities (for refining, ammonia, methanol and steel production). This is notable as $H_2$ release from $H_2$ produc-
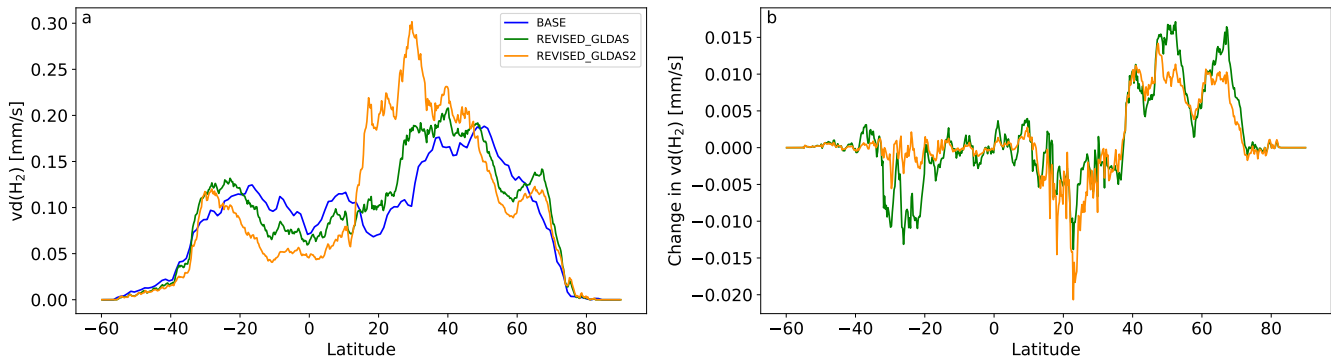
**Figure 7.** Meridional distribution of $v_d(H_2)$ in the BASE, REVISED_GLDAS, and REVISED_GLDAS2 simulations (a) and (b) simulated change in $v_d(H_2)$ between (2017–2019) and (2010-2012)
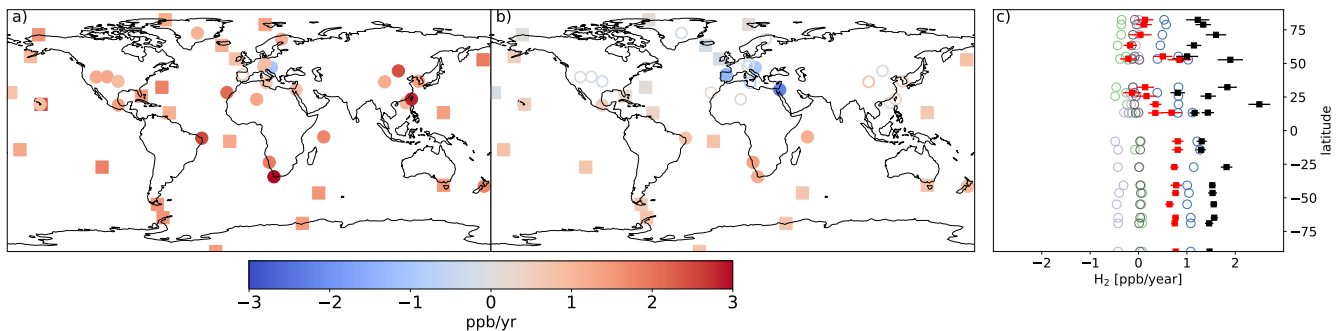
**Figure 8.** Same as Fig. 4 but for the REVISED_GLDAS configuration

tion facilities is poorly understood yet important to assess the climate benefits of $H_2$ (Hauglustaine et al., 2022; Bertagni et al., 2022).

We show that the observed trend, seasonality, and meridional gradient of $H_2$ provide complementary constraints on the global $H_2$ biogeochemical cycle. We find that our model fails to capture all three constraints together, which likely reflects fundamental gaps in our representation of the soil removal of $H_2$ by microorganisms (HA-HOB). Such uncertainties are important as an increase in $v_d(H_2)$ would require a commensurate increase in $H_2$ sources to explain the observed change in $H_2$ concentration.

This study highlights the need for coordinated field and laboratory data collection efforts to help improve models of the distribution and activity of HA-HOB in global models (American Academy of Microbiology, 2023). Such work is critical to quantify the response of atmospheric $H_2$ to increasing anthropogenic $H_2$ usage as well as hydrological changes associated with climate change (Jansson and Hofmockel, 2019; Huang et al., 2015) but is hindered by the lack of sensors that offer higher time resolution and maintain good sensitivity and stable response.
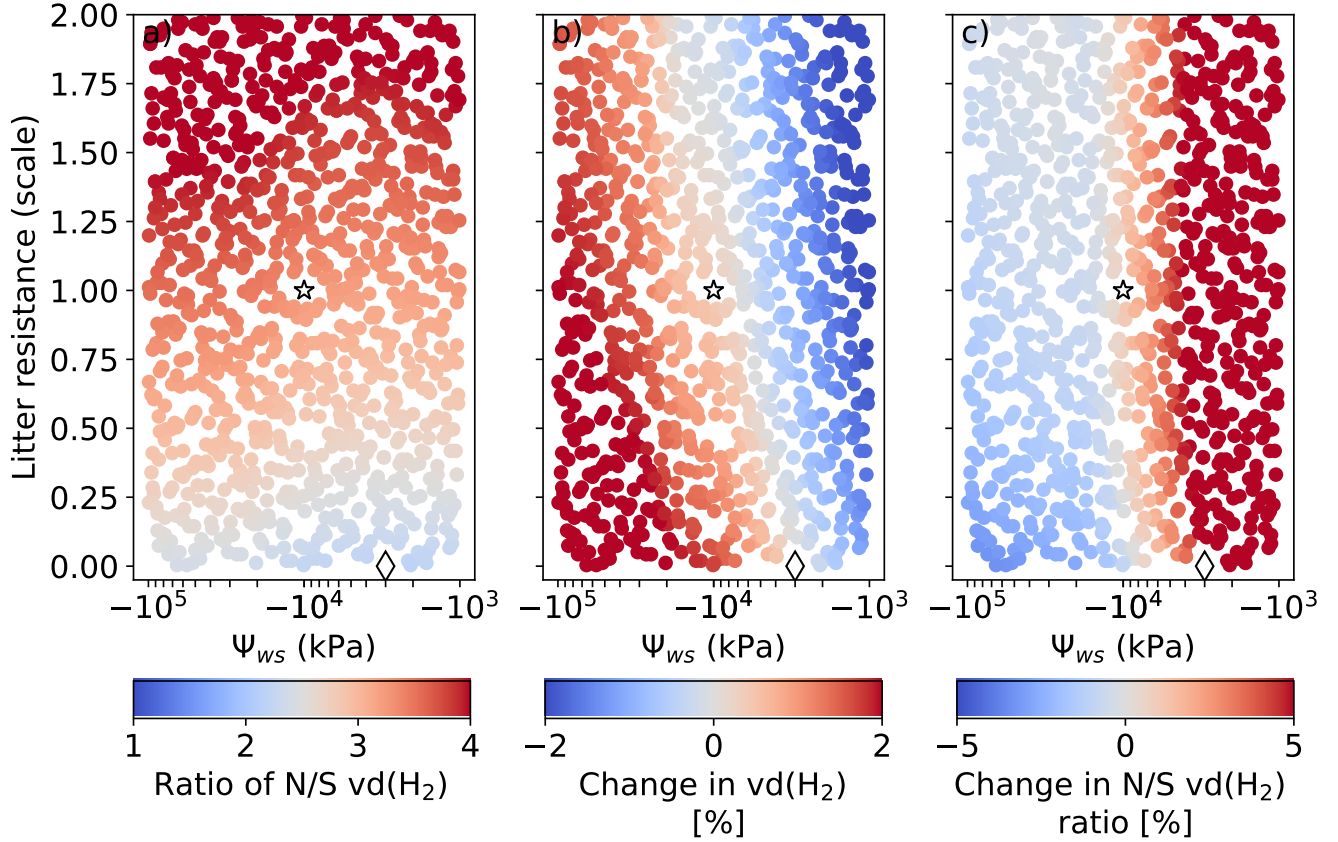
**Figure 9.** Simulated sensitivity of $v_d(\mathrm{H}_2)$ to $\Psi_{ws}$ and the strength of the litter diffusive barrier. Panels a, b and c show the response of the North/South ratio of $v_d(\mathrm{H}_2)$, the difference in $v_d(\mathrm{H}_2)$ in (2017–2019) relative to (2010-2012), and the difference in the N/S $v_d(\mathrm{H}_2)$ gradient in (2017–2019) relative to (2010-2012), respectively. The REVISED_GLDAS configuration uses $\Psi_{ws} = -3000$ kPa and no litter resistance (diamond). The REVISED_GLDAS2 uses $\Psi_{ws} = -10000$ kPa and the default (scale=1) litter resistance (star). The litter scale reflects the perturbation to the default litter resistance (see Text S1.4)

*Code and data availability.* The code for the GFDL ESM4.1 model is available at https://zenodo.org/record/3836405. NOAA Global Cooperative Network Flask Air $H_2$ (Pétron et al., 2023) can be downloaded at https://doi.org/10.15138/WP0W-EZ08.

*Author contributions.* FP designed the research, developed, and analyzed the model simulations. GP and AC collected and processed $H_2$ observations from the NOAA network and provided guidance regarding their interpretation. MB developed the soil moisture parameteri-
275   zation of HA-HOB used in the REVISED_GLDAS and REVISED_GLDAS2 configurations. All authors contributed to the drafting of the manuscript.

*Competing interests.* None

*Acknowledgements.* We thank Vaishali Naik for her help with generating model-ready $H_2$ emissions. We thank Larry Horowitz, Vaishali Naik, Amilcare Porporato, and Xinning Zhang for their helpful comments on the manuscript. This research was supported in part by NOAA
280   cooperative agreements NA17OAR4320101 and NA22OAR4320151 and by the U.S. Department of Energy, Office of Energy Efficiency and Renewable Energy (EERE), specifically the Hydrogen and Fuel Cell Technologies Office. The views expressed herein do not necessarily represent the views of the U.S. Department of Energy or the United States Government.

# References

Abe, J., Popoola, A., Ajenifuja, E., and Popoola, O.: Hydrogen energy, economy and storage: Review and recommendation, International Journal of Hydrogen Energy, 44, 15 072–15 086, https://doi.org/10.1016/j.ijhydene.2019.04.068, 2019.

Akagi, S. K., Yokelson, R. J., Wiedinmyer, C., Alvarado, M. J., Reid, J. S., Karl, T., Crounse, J. D., and Wennberg, P. O.: Emission factors for open and domestic biomass burning for use in atmospheric models, Atmos. Chem. Phys., 11, 4039–4072, https://doi.org/10.5194/acp-11-4039-2011, 2011.

American Academy of Microbiology: Microbes in Models: Integrating Microbes into Earth System Models for Understanding Climate Change: Report on an American Academy of Microbiology Virtual Colloquium held on Dec. 6 and 8, 2022 Washington (DC), 2023.

Andreae, M. O.: Emission of trace gases and aerosols from biomass burning – an updated assessment, Atmospheric Chemistry and Physics, 19, 8523–8546, https://doi.org/10.5194/acp-19-8523-2019, 2019.

Arthur, D. and Vassilvitskii, S.: K-means++: The advantages of careful seeding, Proceedings of the eighteenth annual ACM-SIAM symposium on discrete algorithm, 2007.

Bay, S. K., Dong, X., Bradley, J. A., Leung, P. M., Grinter, R., Jirapanjawat, T., Arndt, S. K., Cook, P. L. M., LaRowe, D. E., Nauer, P. A., Chiri, E., and Greening, C.: Trace gas oxidizers are widespread and active members of soil microbial communities, Nature Microbiology, 6, 246–256, https://doi.org/10.1038/s41564-020-00811-w, 2021.

Bertagni, M. B., Paulot, F., and Porporato, A.: Moisture Fluctuations Modulate Abiotic and Biotic Limitations of $H_2$ Soil Uptake, Global Biogeochemical Cycles, 35, https://doi.org/10.1029/2021gb006987, 2021.

Bertagni, M. B., Pacala, S. W., Paulot, F., and Porporato, A.: Risk of the hydrogen economy for atmospheric methane, Nature Communications, 13, https://doi.org/10.1038/s41467-022-35419-7, 2022.

Constant, P., Poissant, L., and Villemur, R.: Isolation of Streptomyces sp. PCB7, the first microorganism demonstrating high-affinity uptake of tropospheric $H_2$, The ISME Journal, 2, 1066–1076, https://doi.org/10.1038/ismej.2008.59, 2008.

da Silva Veras, T., Mozer, T. S., da Costa Rubim Messeder dos Santos, D., and da Silva César, A.: Hydrogen: Trends, production and characterization of the main process worldwide, International Journal of Hydrogen Energy, 42, 2018–2033, https://doi.org/10.1016/j.ijhydene.2016.08.219, 2017.

Dawood, F., Anda, M., and Shafiullah, G.: Hydrogen production for energy: An overview, International Journal of Hydrogen Energy, 45, 3847–3869, https://doi.org/10.1016/j.ijhydene.2019.12.059, 2020.

Derwent, R. G., Collins, W. J., Johnson, C. E., and Stevenson, D. S.: Transient Behaviour of Tropospheric Ozone Precursors in a Global 3-D CTM and Their Indirect Greenhouse Effects, Climatic Change, 49, 463–487, https://doi.org/10.1023/a:1010648913655, 2001.

Derwent, R. G., Simmonds, P. G., Doherty, S. J. O., Spain, T. G., and Young, D.: Natural greenhouse gas and ozone-depleting substance sources and sinks from the peat bogs of Connemara, Ireland from 1994–2020, Environmental Science: Atmospheres, 1, 406–415, https://doi.org/10.1039/d1ea00040c, 2021.

Derwent, R. G., Simmonds, P. G., O'Doherty, S., Manning, A. J., and Spain, T. G.: High-frequency, continuous hydrogen observations at Mace Head, Ireland from 1994 to 2022: Baselines, pollution events and 'missing' sources, Atmospheric Environment, 312, 120 029, https://doi.org/10.1016/j.atmosenv.2023.120029, 2023.

Dunne, J. P., Horowitz, L. W., Adcroft, A. J., Ginoux, P., Held, I. M., John, J. G., Krasting, J. P., Malyshev, S., Naik, V., Paulot, F., Shevliakova, E., Stock, C. A., Zadeh, N., Balaji, V., Blanton, C., Dunne, K. A., Dupuis, C., Durachta, J., Dussin, R., Gauthier, P. P. G., Griffies, S. M., Guo, H., Hallberg, R. W., Harrison, M., He, J., Hurlin, W., McHugh, C., Menzel, R., Milly, P. C. D., Nikonov, S., Paynter, D. J., Ploshay, J.,

320  Radhakrishnan, A., Rand, K., Reichl, B. G., Robinson, T., Schwarzkopf, D. M., Sentman, L. T., Underwood, S., Vahlenkamp, H., Winton, M., Wittenberg, A. T., Wyman, B., Zeng, Y., and Zhao, M.: The GFDL Earth System Model version 4.1 (GFDL-ESM 4.1): Overall coupled model description and simulation characteristics, Journal of Advances in Modeling Earth Systems, https://doi.org/10.1029/2019ms002015, 2020.

Ehhalt, D. and Rohrer, F.: Deposition velocity of $H_2$: a new algorithm for its dependence on soil moisture and temperature, Tellus B: Chemical

325  and Physical Meteorology, 65, 19 904, https://doi.org/10.3402/tellusb.v65i0.19904, 2013.

Ehhalt, D. H. and Rohrer, F.: The tropospheric cycle of $H_2$: a critical review, Tellus B: Chemical and Physical Meteorology, 61, 500–535, https://doi.org/10.1111/j.1600-0889.2009.00416.x, 2009.

Francey, R. J., Steele, L. P., Spencer, D. A., Langenfelds, R. L., Law, R. M., Krummel, P. B., Fraser, P. J., Etheridge, D. M., Derek, N., Coram, S. A., Cooper, L. N., Allison, C. E., Porter, L., and Baly, S.: The CSIRO (Australia) measurement of greenhouse gases in the

330  global atmosphere., Tech. rep., http://hdl.handle.net/102.100.100/191835?index=1, 2003.

Ghosh, A., Patra, P. K., Ishijima, K., Umezawa, T., Ito, A., Etheridge, D. M., Sugawara, S., Kawamura, K., Miller, J. B., Dlugokencky, E. J., Krummel, P. B., Fraser, P. J., Steele, L. P., Langenfelds, R. L., Trudinger, C. M., White, J. W. C., Vaughn, B., Saeki, T., Aoki, S., and Nakazawa, T.: Variations in global methane sources and sinks during 1910–2010, Atmospheric Chemistry and Physics, 15, 2595–2612, https://doi.org/10.5194/acp-15-2595-2015, 2015.

335  Global Monitoring Laboratory: Carbon Cycle Gases observation sites, https://www.gml.noaa.gov/dv/site/?program=ccgg, 2023.

Granier, C., Lamarque, J. F., Mieville, A., Müller, J. F., Olivier, J., Orlando, J., Peters, J., Petron, G., Tyndall, G., and Wallens, S.: POET, a database of surface emissions of ozone precursors, available on internet at http://www.aero.jussieu.fr/projet/ACCENT/POET.php, Tech. rep., 2005.

Grant, A., Archibald, A. T., Cooke, M. C., Nickless, G., and Shallcross, D. E.: Modelling the oxidation of 15 VOCs to track yields of

340  hydrogen, Atmospheric Science Letters, 11, 265–269, https://doi.org/10.1002/asl.286, 2010.

Greening, C. and Grinter, R.: Microbial oxidation of atmospheric trace gases, Nature Reviews Microbiology, 20, 513–528, https://doi.org/10.1038/s41579-022-00724-x, 2022.

Greening, C., Constant, P., Hards, K., Morales, S. E., Oakeshott, J. G., Russell, R. J., Taylor, M. C., Berney, M., Conrad, R., and Cook, G. M.: Atmospheric Hydrogen Scavenging: from Enzymes to Ecosystems, Applied and Environmental Microbiology, 81, 1190–1199,

345  https://doi.org/10.1128/aem.03364-14, 2015.

Guenther, A. B., Jiang, X., Heald, C. L., Sakulyanontvittaya, T., Duhl, T., Emmons, L. K., and Wang, X.: The Model of Emissions of Gases and Aerosols from Nature version 2.1 (MEGAN2.1): an extended and updated framework for modeling biogenic emissions, Geoscientific Model Development, 5, 1471–1492, https://doi.org/10.5194/gmd-5-1471-2012, 2012.

Hauglustaine, D., Paulot, F., Collins, W., Derwent, R., Sand, M., and Boucher, O.: Climate benefit of a future hydrogen economy, Commu-

350  nications Earth & Environment, 3, https://doi.org/10.1038/s43247-022-00626-z, 2022.

Holladay, J., Hu, J., King, D., and Wang, Y.: An overview of hydrogen production technologies, Catalysis Today, 139, 244–260, https://doi.org/10.1016/j.cattod.2008.08.039, 2009.

Horowitz, L. W., Naik, V., Paulot, F., Ginoux, P. A., Dunne, J. P., Mao, J., Schnell, J., Chen, X., He, J., John, J. G., Lin, M., Lin, P., Malyshev, S., Paynter, D., Shevliakova, E., and Zhao, M.: The GFDL Global Atmospheric Chemistry-Climate Model AM4.1: Model Description

355  and Simulation Characteristics, Journal of Advances in Modeling Earth Systems, https://doi.org/10.1029/2019ms002032, 2020.

Howarth, R. W. and Jacobson, M. Z.: How green is blue hydrogen?, Energy Science & Engineering, 9, 1676–1687, https://doi.org/10.1002/ese3.956, 2021.

Huang, J., Yu, H., Guan, X., Wang, G., and Guo, R.: Accelerated dryland expansion under climate change, Nature Climate Change, 6, 166–171, https://doi.org/10.1038/nclimate2837, 2015.

360 Hydrogen Council: Hydrogen scaling up. A sustainable pathway for the global energy transition, 2017.

International Energy Agency: The Future of Hydrogen – Seizing today's opportunities, Tech. rep., International Energy Agency, Paris, France, 2019.

International Energy Agency: Global Hydrogen Review 2022, Tech. rep., International Energy Agency, Paris, France, 2022.

Jansson, J. K. and Hofmockel, K. S.: Soil microbiomes and climate change, Nature Reviews Microbiology, 18, 35–46,
365 https://doi.org/10.1038/s41579-019-0265-7, 2019.

Jordaan, K., Lappan, R., Dong, X., Aitkenhead, I. J., Bay, S. K., Chiri, E., Wieler, N., Meredith, L. K., Cowan, D. A., Chown, S. L., and Greening, C.: Hydrogen-Oxidizing Bacteria Are Abundant in Desert Soils and Strongly Stimulated by Hydration, mSystems, 5, https://doi.org/10.1128/msystems.01131-20, 2020.

Jordan, A. and Steinberg, B.: Calibration of atmospheric hydrogen measurements, Atmospheric Measurement Techniques, 4, 509–521,
370 https://doi.org/10.5194/amt-4-509-2011, 2011.

Kalnay, E., Kanamitsu, M., Kistler, R., Collins, W., Deaven, D., Gandin, L., Iredell, M., Saha, S., White, G., Woollen, J., Zhu, Y., Leetmaa, A., Reynolds, R., Chelliah, M., Ebisuzaki, W., Higgins, W., Janowiak, J., Mo, K. C., Ropelewski, C., Wang, J., Jenne, R., and Joseph, D.: The NCEP/NCAR 40-Year Reanalysis Project, Bull. Am. Meteorol. Soc., 77, 437–471, 1996.

Khdhiri, M., Hesse, L., Popa, M. E., Quiza, L., Lalonde, I., Meredith, L. K., Röckmann, T., and Constant, P.: Soil carbon content and
375 relative abundance of high affinity $H_2$-oxidizing bacteria predict atmospheric $H_2$ soil uptake activity better than soil microbial community composition, Soil Biology and Biochemistry, 85, 1–9, https://doi.org/10.1016/j.soilbio.2015.02.030, 2015.

Lapi, T., Chatzimpiros, P., Raineau, L., and Prinzhofer, A.: System approach to natural versus manufactured hydrogen: An interdisciplinary perspective on a new primary energy source, International Journal of Hydrogen Energy, 47, 21701–21712, https://doi.org/10.1016/j.ijhydene.2022.05.039, 2022.

380 Lefeuvre, N., Truche, L., Donzé, F., Ducoux, M., Barré, G., Fakoury, R., Calassou, S., and Gaucher, E. C.: Native H2 Exploration in the Western Pyrenean Foothills, Geochemistry, Geophysics, Geosystems, 22, https://doi.org/10.1029/2021gc009917, 2021.

Li, J., Mao, J., Min, K.-E., Washenfelder, R. A., Brown, S. S., Kaiser, J., Keutsch, F. N., Volkamer, R., Wolfe, G. M., Hanisco, T. F., Pollack, I. B., Ryerson, T. B., Graus, M., Gilman, J. B., Lerner, B. M., Warneke, C., de Gouw, J. A., Middlebrook, A. M., Liao, J., Welti, A., Henderson, B. H., McNeill, V. F., Hall, S. R., Ullmann, K., Donner, L. J., Paulot, F., and Horowitz, L. W.: Observational constraints on
385 glyoxal production from isoprene oxidation and its contribution to organic aerosol over the Southeast United States, J. Geophys. Res. Atmos., 121, 9849–9861, https://doi.org/10.1002/2016JD025331, 2016JD025331, 2016.

Meinshausen, M., Vogel, E., Nauels, A., Lorbacher, K., Meinshausen, N., Etheridge, D. M., Fraser, P. J., Montzka, S. A., Rayner, P. J., Trudinger, C. M., Krummel, P. B., Beyerle, U., Canadell, J. G., Daniel, J. S., Enting, I. G., Law, R. M., Lunder, C. R., O'Doherty, S., Prinn, R. G., Reimann, S., Rubino, M., Velders, G. J. M., Vollmer, M. K., Wang, R. H. J., and Weiss, R.: Historical greenhouse gas concentrations
390 for climate modelling (CMIP6), Geoscientific Model Development, 10, 2057–2116, https://doi.org/10.5194/gmd-10-2057-2017, 2017.

Meinshausen, M., Nicholls, Z. R. J., Lewis, J., Gidden, M. J., Vogel, E., Freund, M., Beyerle, U., Gessner, C., Nauels, A., Bauer, N., Canadell, J. G., Daniel, J. S., John, A., Krummel, P. B., Luderer, G., Meinshausen, N., Montzka, S. A., Rayner, P. J., Reimann, S., Smith, S. J., van den Berg, M., Velders, G. J. M., Vollmer, M. K., and Wang, R. H. J.: The shared socio-economic pathway (SSP) greenhouse gas concentrations and their extensions to 2500, Geoscientific Model Development, 13, 3571–3605, https://doi.org/10.5194/gmd-13-3571-2020, 2020.

395    Meredith, L. K., Commane, R., Keenan, T. F., Klosterman, S. T., Munger, J. W., Templer, P. H., Tang, J., Wofsy, S. C., and Prinn, R. G.: Ecosystem fluxes of hydrogen in a mid-latitude forest driven by soil microorganisms and plants, Global Change Biology, 23, 906–919, https://doi.org/10.1111/gcb.13463, 2016.

Milkov, A. V.: Molecular hydrogen in surface and subsurface natural gases: Abundance, origins and ideas for deliberate exploration, Earth-Science Reviews, 230, 104 063, https://doi.org/10.1016/j.earscirev.2022.104063, 2022.

400    Ocko, I. B. and Hamburg, S. P.: Climate consequences of hydrogen emissions, Atmospheric Chemistry and Physics, 22, 9349–9368, https://doi.org/10.5194/acp-22-9349-2022, 2022.

O'Rourke, P., Smith, S., Mott, A., Ahsan, H., Mcduffie, E., Crippa, M., Klimont, Z., Mcdonald, B., Wang, S., Nicholson, M., Hoesly, R., and Feng, L.: CEDS v_2021_04_21 Gridded emissions data, https://doi.org/10.25584/PNNLDATAHUB/1779095, 2021.

Paulot, F., Paynter, D., Naik, V., Malyshev, S., Menzel, R., and Horowitz, L. W.: Global modeling of hydrogen using GFDL-
405    AM4.1: Sensitivity of soil removal and radiative forcing, International Journal of Hydrogen Energy, 46, 13 446–13 460, https://doi.org/10.1016/j.ijhydene.2021.01.088, 2021.

Pétron, G., Crotwell, A., Crotwell, M., Kitzis, D., Madronich, M., Mefford, T., Moglia, E., Mund, J., Neff, D., Thoning, K., and Wolter, S.: Atmospheric Hydrogen Dry Air Mole Fractions from the NOAA GML Carbon Cycle Cooperative Global Air Sampling Network, 2009-Present, https://doi.org/10.15138/WP0W-EZ08, 2023.

410    Pétron, G., Crotwell, A., Mund, J., Crotwell, M., Mefford, T., Thoning, K., Hall, B., Kitzis, D., Madronich, M., Moglia, E., Neff, D., Wolter, S., Jordan, A., Krummel, P., Langenfeld, R., Patterson, J. D., and Andrews, A.: Atmospheric $H_2$ observations from the NOAA Global Greenhouse Gas Reference Network, Atmospheric Measurement Techniques, submitted.

Price, H., Jaeglé, L., Rice, A., Quay, P., Novelli, P. C., and Gammon, R.: Global budget of molecular hydrogen and its deuterium content: Constraints from ground station, cruise, and aircraft observations, Journal of Geophysical Research, 112,
415    https://doi.org/10.1029/2006jd008152, 2007.

Prinn, R. G., Weiss, R. F., Arduini, J., Arnold, T., DeWitt, H. L., Fraser, P. J., Ganesan, A. L., Gasore, J., Harth, C. M., Hermansen, O., and et al.: History of chemically and radiatively important atmospheric gases from the Advanced Global Atmospheric Gases Experiment (AGAGE), Earth System Science Data, 10, 985–1018, https://doi.org/10.5194/essd-10-985-2018, 2018.

Prinzhofer, A., Cissé, C. S. T., and Diallo, A. B.: Discovery of a large accumulation of natural hydrogen in Bourakebougou (Mali), Interna-
420    tional Journal of Hydrogen Energy, 43, 19 315–19 326, https://doi.org/10.1016/j.ijhydene.2018.08.193, 2018.

Rayner, N. A., Parker, D. E., Horton, E. B., Folland, C. K., Alexander, L. V., Rowell, D. P., Kent, E. C., and Kaplan, A.: Global analyses of sea surface temperature, sea ice, and night marine air temperature since the late nineteenth century, J. Geophys. Res. Atmos., 108, 4407, https://doi.org/10.1029/2002JD002670, 2003.

Rodell, M., Houser, P. R., Jambor, U., Gottschalck, J., Mitchell, K., Meng, C.-J., Arsenault, K., Cosgrove, B., Radakovich, J., Bosilovich, M.,
425    Entin, J. K., Walker, J. P., Lohmann, D., and Toll, D.: The Global Land Data Assimilation System, Bulletin of the American Meteorological Society, 85, 381–394, https://doi.org/10.1175/bams-85-3-381, 2004.

Röth, E.-P. and Ehhalt, D. H.: A simple formulation of the $CH_2O$ photolysis quantum yields, Atmospheric Chemistry and Physics, 15, 7195–7202, https://doi.org/10.5194/acp-15-7195-2015, 2015.

Sand, M., Skeie, R. B., Sandstad, M., Krishnan, S., Myhre, G., Bryant, H., Derwent, R., Hauglustaine, D., Paulot, F., Prather, M., and
430    Stevenson, D.: A multi-model assessment of the Global Warming Potential of hydrogen, Communications Earth & Environment, 4, https://doi.org/10.1038/s43247-023-00857-8, 2023.

Saunois, M., Stavert, A. R., Poulter, B., Bousquet, P., Canadell, J. G., Jackson, R. B., Raymond, P. A., Dlugokencky, E. J., Houweling, S., Patra, P. K., Ciais, P., Arora, V. K., Bastviken, D., Bergamaschi, P., Blake, D. R., Brailsford, G., Bruhwiler, L., Carlson, K. M., Carrol, M., Castaldi, S., Chandra, N., Crevoisier, C., Crill, P. M., Covey, K., Curry, C. L., Etiope, G., Frankenberg, C., Gedney, N., Hegglin, M. I., Höglund-Isaksson, L., Hugelius, G., Ishizawa, M., Ito, A., Janssens-Maenhout, G., Jensen, K. M., Joos, F., Kleinen, T., Krummel, P. B., Langenfelds, R. L., Laruelle, G. G., Liu, L., Machida, T., Maksyutov, S., McDonald, K. C., McNorton, J., Miller, P. A., Melton, J. R., Morino, I., Müller, J., Murguia-Flores, F., Naik, V., Niwa, Y., Noce, S., O'Doherty, S., Parker, R. J., Peng, C., Peng, S., Peters, G. P., Prigent, C., Prinn, R., Ramonet, M., Regnier, P., Riley, W. J., Rosentreter, J. A., Segers, A., Simpson, I. J., Shi, H., Smith, S. J., Steele, L. P., Thornton, B. F., Tian, H., Tohjima, Y., Tubiello, F. N., Tsuruta, A., Viovy, N., Voulgarakis, A., Weber, T. S., van Weele, M., van der Werf, G. R., Weiss, R. F., Worthy, D., Wunch, D., Yin, Y., Yoshida, Y., Zhang, W., Zhang, Z., Zhao, Y., Zheng, B., Zhu, Q., Zhu, Q., and Zhuang, Q.: The Global Methane Budget 2000–2017, Earth System Science Data, 12, 1561–1623, https://doi.org/10.5194/essd-12-1561-2020, 2020.

Smith-Downey, N. V., Randerson, J. T., and Eiler, J. M.: Temperature and moisture dependence of soil $H_2$ uptake measured in the laboratory, Geophysical Research Letters, 33, https://doi.org/10.1029/2006gl026749, 2006.

Smith-Downey, N. V., Randerson, J. T., and Eiler, J. M.: Molecular hydrogen uptake by soils in forest, desert, and marsh ecosystems in California, Journal of Geophysical Research, 113, https://doi.org/10.1029/2008jg000701, 2008.

Staffell, I., Scamman, D., Abad, A. V., Balcombe, P., Dodds, P. E., Ekins, P., Shah, N., and Ward, K. R.: The role of hydrogen and fuel cells in the global energy system, Energy & Environmental Science, 12, 463–491, https://doi.org/10.1039/c8ee01157e, 2019.

Taylor, K. E., Williamson, D., and Zwiers, F.: The sea surface temperature and sea-ice concentration boundary conditions for AMIP II simulations, Program for Climate Model Diagnosis and Intercomparison, Lawrence Livermore National Laboratory, University of California, 2000.

van der Werf, G. R., Randerson, J. T., Giglio, L., Collatz, G. J., Kasibhatla, P. S., and Arellano, A. F.: Interannual variability in global biomass burning emissions from 1997 to 2004, Atmospheric Chemistry and Physics, 6, 3423–3441, https://doi.org/10.5194/acp-6-3423-2006, 2006.

van der Werf, G. R., Randerson, J. T., Giglio, L., van Leeuwen, T. T., Chen, Y., Roḡers, B. M., Mu, M., van Marle, M. J. E., Morton, D. C., Collatz, G. J., Yokelson, R. J., and Ǩasibhatla, P. S.: Global fire emissions estimates during 1997–2016, Earth System Science Data, 9, 697–720, https://doi.org/10.5194/essd-9-697-2017, 2017.

WMO: WMO Greenhouse Gas Bulletin, Tech. Rep. 17, Japan Meterological Agency and WMO, 2021.

Yashiro, H., Sudo, K., Yonemura, S., and Takigawa, M.: The impact of soil uptake on the global distribution of molecular hydrogen: chemical transport model simulation, Atmospheric Chemistry and Physics, 11, 6701–6719, https://doi.org/10.5194/acp-11-6701-2011, 2011.

Zgonnik, V.: The occurrence and geoscience of natural hydrogen: A comprehensive review, Earth-Science Reviews, 203, 103 140, https://doi.org/10.1016/j.earscirev.2020.103140, 2020.